chemosensors

MDPI

Article

Au-Decorated WS_2 Microflakes Based Sensors for Selective Ammonia Detection at Room Temperature

Qiyilan Guang, Baoyu Huang * and Xiaogan Li *

School of Microelectronics, Dalian University of Technology, Dalian 116024, China; guangqiyilan@mail.dlut.edu.cn
* Correspondence: huangby@dlut.edu.cn (B.H.); lixg@dlut.edu.cn (X.L.)

Abstract: Gold nanoparticles decorated WS_2 microflakes (Au/WS_2) have been synthesized by an in situ chemical reducing process. A chemiresistive-type sensor using as-synthesized Au/WS_2 heterostructures as sensing materials shows an improved response to different concentrations of ammonia compared to pure WS_2 at room temperature. As the concentrations of gold nanoparticles increased in heterostructures, response/recovery speeds of the sensors became faster although the sensitivity of the sensor was compromised compared to the sensitivity of the sensor with lower concentrations of Au. In addition, the Au/WS_2-based sensor indicated excellent selectivity to formaldehyde, ethanol, benzene and acetone at room temperature. The improved performance of the sensors was attributed to the synergistic effect of electronic sensitization and chemical sensitization between WS_2 and Au.

Keywords: Au-decorated WS_2 microflakes; chemical gas sensors; NH_3

Citation: Guang, Y.; Huang, B.; Li, X. Au-Decorated WS_2 Microflakes Based Sensors for Selective Ammonia Detection at Room Temperature. *Chemosensors* **2022**, *10*, 9. https://doi.org/10.3390/chemosensors10010009

Academic Editors: Qu Zhou, Wen Zeng and Zhongchang Wang

Received: 21 November 2021
Accepted: 22 December 2021
Published: 27 December 2021

1. Introduction

Ammonia is a natural gas existing throughout the atmosphere that is used extensively in many areas such as fertilizers, chemical technology and environmental protection [1]. The demand for fuel combustion efficiency and strict regulations on automobile exhaust emissions result in an urgent need for new exhaust gas treatment methods such as ammonia selective catalytic NO_x reduction (SCR) [2]. Toxic NO_x could be reduced effectively by NH_3, which has been used for lowering emissions [3]. However, since ammonia is a toxic gas that is harmful to human health, and the concentration of ammonia injected into the atmosphere should be controlled in order to avoid environmental pollution and damage to human health. Therefore, the concentration of ammonia in the exhaust system needs to be detected to optimize emissions [4]. In these circumstances, there is an increasing need of ammonia sensors with good sensing performances in these fields.

Due to the need of low cost and low energy consumption, ammonia sensors working at low working temperature with high sensitivity, simplicity, and compatibility with miniaturized electronic devices are in high demand. As the core component of the sensor, sensing materials are key factors affecting sensing performance. Therefore, selecting appropriate sensing materials that can work at room temperature is an effective means to reduce energy consumption of the sensor [5–8]. Two-dimensional (2D) materials such as graphene and other 2D transitional metal dichalcogenides (TMDs) with graphene-like structures have become potential candidates for meeting such requirements for chemical gas sensors [9–11]. According to the reported studies, the 2D materials have been widely used in a variety of fields, and they are expected to be used in next-generation nanoelectronic devices [12–17]. Based on the sensing mechanism of semiconductor gas sensors, 2D material has highly specific surface areas and can provide sufficient active sites, which is conducive to the adsorption of gas molecules on the surface of sensitive materials so as to realize the improvement of sensing performance [18–22]. Due to its unique electronic transport properties, graphene has become the most concerned 2D material and has been

widely studied. However, the band gap of pristine graphene is zero, which is an essential characteristic in many applications, resulting in its application being limited [23,24]. TMDs materials not only have excellent electrical properties similar to graphene but also have semiconductor energy band structure, which have been considered to be a promising sensing material. In the TMDs family, MoS_2 and WS_2 as typical 2D materials have attracted the most attention because of their wider band gap structure (1–3 eV) and excellent physical and chemical properties [25–27]. In particular, relative to WS_2 based chemical gas sensors, Li et al. fabricated an ammonia gas sensor used WS_2 nanoflakes as the sensing material, which can work at room temperature and displayed high selectivity to ammonia gas [28]. Gu developed a gas sensor based on WS_2 microflakes and found that the fabricated sensor showed better sensitivity and selectivity to ammonia gas under different light illumination compared to those in the dark [29].

In order to further improve the sensing performance of WS_2 based chemiresistive-type sensor, secondary additives such as metallic nanoparticles was introduced. Chao investigated the gas sensor based on WS_2 nanosheets modified by Pt quantum dots (QDs) and found that the sensor indicated enhanced sensing properties and fast recovery speeds to ammonia, which is attributed to the extra charges transferred from noble metal Pt QDs to WS_2 nanosheets induced by unbalanced Fermi levels at the interfaces [30]. Zhang et al. reported that Cu doped WS_2 displayed good sensing properties for CO and NO gases suitable for NO_2 gas scavenger, while it was not suitable for CO_2 gas sensing [18]. Xu et al. demonstrated a NO_2 sensor that used WS_2 nanosheets/carbon nanofibers (CNFs) composites as the sensing material, which can significantly enhance sensing performances relative to NO_2 at room temperature [31]. More interestingly, Suh et al. assembled WS_2 particles on porous SiO_2 nanorods templates with numerous edge-exposed WS_2 microflakes and the resulting sensor exhibited a high sensitivity relative to NO_2 at room temperature [32]. The introduced secondary phase could enhance both sensitivity and response speeds through mechanisms such as electronic sensitization or chemical sensitization [33,34].

In this study, we synthesized Au/WS_2 nanocomposites via in situ reduction processes and examined the effect of introduced Au nanoparticles on the sensing properties relative to NH_3 at room temperatures. The gas sensor based on the as-prepared Au/WS_2 nanocomposites displayed a higher response value and faster response and recovery properties compared to those of the pristine one, indicating a significantly improved gas sensing performance to ammonia. Moreover, with Au introduction, the sensor could even work in high humidity backgrounds exhibiting a potential application in exhaled breath gas-phase analysis.

2. Experimental Method

2.1. Synthesis of Au/WS_2 Nanocomposites

Commercial WS_2 powders were purchased from Aladdin Co., Shanghai, China. In this research study, all chemical reagents are analytically pure and did not undergo further purification. In typical synthesis, 50 mg of WS_2 microflakes was added in 15 mL deionized water followed with ultrasonication for 15 min to form a homogeneous mixed solution. A certain amount (0.1 mL, 0.2 mL, 0.6 mL and 1 mL, respectively) of aqueous solution of chlorauric acid ($HAuCl_4$) with concentrations of 0.01 M and a corresponding amount (0.1 mL, 0.2 mL, 0.6 mL and 1 mL, respectively) of L-lysine solution ($C_{11}H_{23}N_3O_6$) with concentrations of 0.01 M were added in the as-prepared solution. L-lysine plays an important role in the bond of Au nanoparticles and WS_2 microflakes. After the above process, different amounts (0.01 mL, 0.02 mL, 0.06 mL and 0.1 mL, respectively) of 0.1 M Na_3cit solution were dropped into the mixture and stirred continuously for 30 min. The obtained precipitate was desiccated at 60 °C for 6 h, which had been washed several times with deionized water and absolute ethanol. For convenience, the samples decorated with different Au concentrations were named as Au/WS_2-0.56, Au/WS_2-1.12, Au/WS_2-3.36 and Au/WS_2-5.6, respectively. The preparation of the sensors is shown in Figure 1.

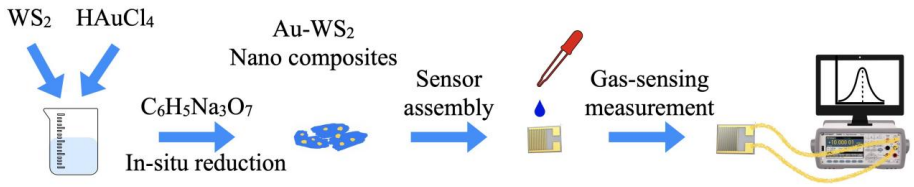

Figure 1. Schematic diagram of synthesis and gas sensing measure of Au/WS_2 nanocomposite-based gas sensor.

2.2. Characterization

In order to investigate the chemical composition and crystallographic structure of WS_2 microflakes and Au/WS_2 nanocomposite-based samples, X-ray diffraction studies were carried out on an X-ray diffractometer (XRD, D8 Advance, Bruker Corporation, Billerica, MA, USA). Field emission scanning electronic microscope (FESEM, Gemini 300, ZEISS Corporation, Jena, Germany) characterization and transmission electron microscope (TEM, Tecnai G2 F20, FEI Corporation, Hillsboro, OR, USA) characterization were used to produce a clear morphology of the WS_2 microflakes and Au/WS_2 nanocomposite-based samples. Energy-dispersive X-ray spectroscopy (EDS) characterization was used to analyze the element's composition of WS_2 microflakes and Au/WS_2 nanocomposite-based samples. X-ray photoelectron spectrometer (XPS, ESCALAB 250Xi, Thermo Fisher Scientific Corporation, Waltham, MA, USA) was used to analyze the surface chemistry of the as-prepared samples.

2.3. Fabrication and Measurement of the Gas Sensors

Pure WS_2 microflakes and the prepared Au/WS_2 nanocomposites were added in a small amount deionized water and ground into a pastes, which were coated on the Al_2O_3 substrate preprinted with Au electrodes to form a gas sensor. In the testing procedure, the as-prepared sensors were placed in a test chamber with a volume of 18 L. After the sensor's resistance stabilized, the target gas obtained by vaporizing the corresponding liquid was injected into the test chamber. The concentration of target gas can be calculated by the following equation.

$$C = (22.4 \times \rho \times d \times V_1)/(M \times V_2) \quad (1)$$

In this equation, C (ppm), ρ (g/mL), d, M (g/mol), V_1 (L) and V_2 (L) represent target gas concentration, liquid density, liquid purity, liquid molecular weight, liquid volume and test chamber volume, respectively.

The digital electromultimeter (Keysight Technologies 34465A, Santa Rosa, CA, USA) was used to measure the resistance of the as-prepared samples. The ratio of the sensor resistances measured in target gas (R_g) and in air (R_a) was used to represent the sensor's response value (R_s). Response time (t_{res}) and recovery time (t_{recov}) were defined as the time required for sensor resistance to change from the initial value to 90% of the full amplitude of resistance change when the target gas is injected and expelled, respectively.

3. Results and Discussion

3.1. Structure and Morphology Characterizations

The XRD patterns of pure WS_2 microflakes and Au-decorated WS_2 nanocomposites are shown in Figure 2. Pure WS_2 microflakes could be indexed to 2H-WS_2 according to PDF#87-2417 with lattice constant of a = 3.16 Å. The XRD patterns of Au/WS_2-1.12 and Au/WS_2-5.6 samples were very similar to the XRD pattern of the WS_2 sample. Moreover, the weak peak shown in the pattern of Au/WS_2-5.6 sample can be ascribed to the crystal plane of (111) of the face-centered cubic (fcc) Au according to PDF#65-8601. However, for the decoration amount of Au in WS_2 microflakes was very small, and the peaks that can

be ascribed to the crystal planes of (200), (220) and (311) of Au cannot be detected in XRD patterns of Au/WS_2-5.6 and Au/WS_2-1.12 with lower Au content.

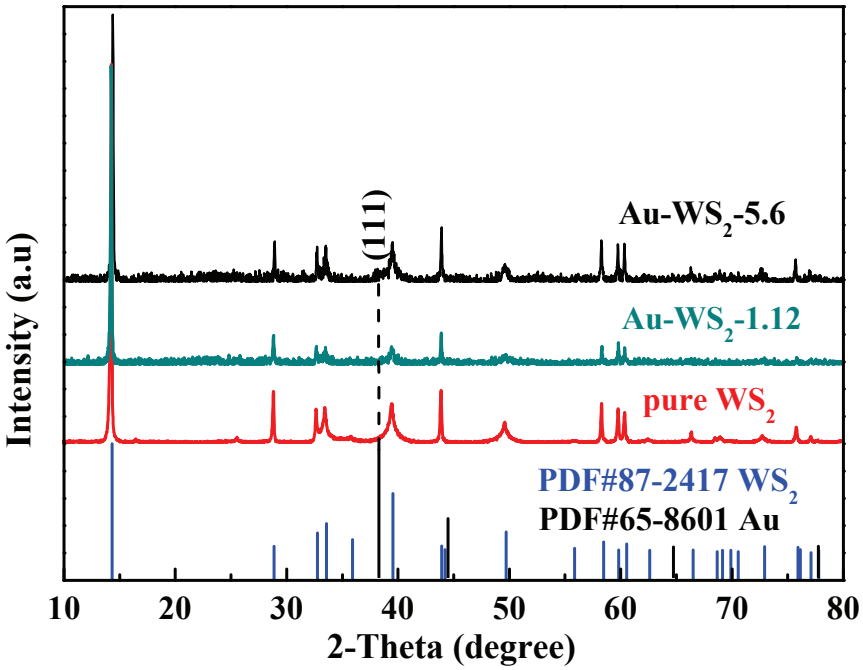

Figure 2. XRD patterns of pure WS_2 and Au/WS_2 based samples.

Figure 3a,b show FESEM images of the surface morphology of pure WS_2 microflakes and Au/WS_2-5.6 nanocomposites. WS_2 and Au/WS_2-5.6 samples both exhibited layered flake morphology indicating the formation of Au nanoparticles that did not result in morphological change of WS_2 microflakes. After Au decoration, WS_2 microflake structure remained unchanged and the formed isolated crystal Au nanoparticles were found to be attached to the surface of WS_2 microflakes in a discrete state, as shown in Figure 3b. Lower magnification SEM images of WS_2 microflakes and Au/WS_2-5.6 nanocomposites are shown in Figure S1 in the Supplementary Materials. The diameters of WS_2 microflakes are 0.4–4.3 micrometers, and the diameters of decorated Au are 17.8–48.8 nm according to the statistical size distribution shown in Figure S2. In order to further investigate the microstructure of gold nanoparticles, high resolution transmission electron microscope (HRTEM) of Au/WS_2-5.6 nanocomposites was conducted and shown in Figure 3c,d. As observed in Figure 3c, the decorated Au nanoparticles present a spherical shape. The HRTEM image in Figure 3d exhibited the lattice fringes of Au/WS_2-5.6 nanocomposites. The intervals of lattice fringes of 0.235 nm and 0.273 nm correspond to the d-spacing of (111) of Au and the d-spacing of (100) of WS_2, respectively, indicating that there are obvious heterostructure interfaces between Au and WS_2. EDS was further obtained to investigate the element composition of Au/WS_2-5.6 nanocomposites. As shown in Figure S3, the elements of W, S, and Au were all identified. All expected elements including S, W and Au with atomic percentages of 65.98%, 33.12% and 0.9%, respectively, can be found in the EDS spectra. Moreover, EDS mapping analyses are presented in Figure S4. All expected elements are present in the mapping images demonstrating the successful formation of Au nanoparticles on WS_2 microflakes.

Figure 4 shows the XPS characterizations of pure WS_2 and Au/WS_2-5.6 samples. As observed from the survey of XPS pattern of the Au/WS_2-5.6 sample as shown in Figure 4a, the peaks identifying Au 4d and Au 4f can be observed, which demonstrates that Au has been successfully introduced on WS_2 microflakes. Figure 4b,c show the refined O 1s core spectra of pure WS_2 microflakes and Au/WS_2-5.6 nanocomposites, respectively. For pure WS_2 microflakes, the peak for O 1s can be deconvoluted into two peaks located at 531.3 eV and 532.4 eV, respectively. The peak at 531.3 eV can be assigned to absorbed

oxygen [35]. The peak at 532.4 eV can be attributed to SO_4^{2-} [29]. Thus, the atomic percentage of absorbed oxygen and SO_4^{2-} is 25.57% and 74.43%, respectively. However, for the Au/WS_2-5.6 sample, the peak for O 1s spectra can also be deconvoluted into two peaks located at 531.3 eV and 532.4 eV attributing to absorbed oxygen and SO_4^{2-}, respectively. The relative atomic percentage of absorbed oxygen and SO_4^{2-} is 45.57% and 54.43%, respectively. This indicates that there is a larger amount of absorbed oxygen on the surface of Au/WS_2-5.6 nanocomposites compared to the pristine WS_2, presumably due to the chemical sensitization effect of Au on the surface of WS_2. The refined core spectra of Au 4f of Au/WS_2-5.6 sample in Figure 4d shows that the two peaks located at 84.45 eV and 88.05 eV correspond to Au $4f_{7/2}$ and Au $4f_{5/2}$, respectively. The binding energy of Au has slightly shifted up to higher energy compared to bulk Au, which could be attributed to the stronger electronic interactions between WS_2 microflakes with Au nanoparticles.

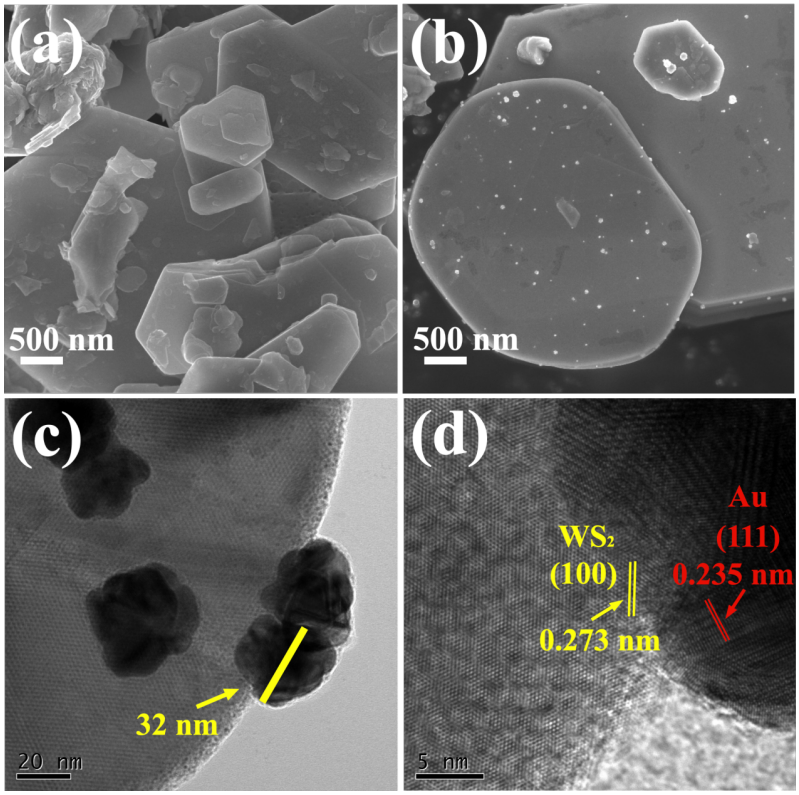

Figure 3. (**a**) FESEM image of pure WS_2 microflakes, (**b**) FESEM image of Au/WS_2-5.6 nanocomposites, (**c**) TEM image of Au/WS_2-5.6 nanocomposites and (**d**) HRTEM image of Au/WS_2-5.6 nanocomposites.

Information on other elements such as W and S is provided in Figure S5a–d in the Supplementary Materials. By performing a comparison on the refined core spectra of S 2p of pure WS_2 and Au/WS_2-5.6 samples, the amount of SO_4^{2-} (169.4 eV of S 2p) was reduced in Au/WS_2-5.6 sample, which confirmed a reduction in the number of SO_4^{2-} after Au decoration. This could be explained by the fact that the slight surface oxidation of WS_2 was inhibited by the reduction agent of Na_3cit used during preparation of the Au/WS_2 nanocomposites. Moreover, as shown in Figure S5a, for the S 2p spectra of WS_2 microflakes, the peaks located at 162.6 eV and 163.8 eV correspond to S $2p_{3/2}$ and S $2p_{1/2}$, respectively. The S 2p spectra of Au/WS_2-5.6 nanocomposites as shown in Figure S5c displays two peaks located at 162.8 eV and 164 eV, which correspond to S $2p_{3/2}$ and S $2p_{1/2}$, respectively. It indicates that sulfide has the valence of -2 both in pure WS_2 microflakes and Au/WS_2-5.6 nanocomposites. The binding energy of S 2p has a slight shift to high energy after Au decoration.

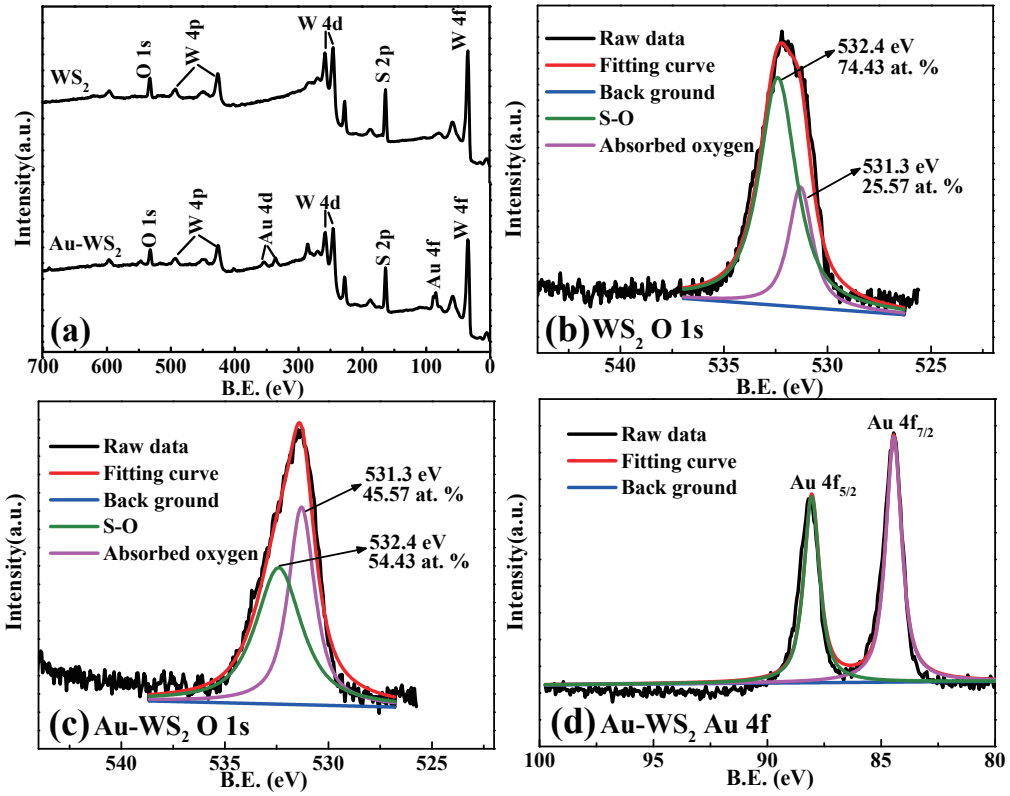

Figure 4. (**a**) XPS spectra of WS_2 microflakes and Au/WS_2-5.6 nanocomposites, (**b**) O 1s of WS_2 microflakes, (**c**) O 1s of Au/WS_2-5.6 nanocomposites and (**d**) Au 4f of Au/WS_2-5.6 nanocomposites.

According to the refined core spectra of the W 4f in WS_2 sample shown in Figure S5b, the two peaks located at 33 eV and 35.2 eV correspond to W $4f_{7/2}$ and W $4f_{5/2}$, respectively. The W 4f spectrum of Au/WS_2-5.6 nanocomposites in Figure S5d exhibits two peaks located at 33.25 eV and 35.45 eV corresponding to W $4f_{7/2}$ and W $4f_{5/2}$, respectively. This indicates that tungsten has the valence of +4 both in WS_2 microflakes and Au/WS_2-5.6 nanocomposites. Therefore, the decoration of Au did not result in a change of chemical oxidation states of S and W in Au/WS_2-5.6 compared to the pristine WS_2. However, the binding energy of S 2p and W 4f had a slight shift to high energy after Au decoration. This could be attributed to the stronger electronic interactions between WS_2 microflakes with Au nanoparticles.

3.2. Electrical and Sensing Performance

Figure 5 shows the polarization curves of the sensors using WS_2 and Au/WS_2 as the sensing materials with a bias voltage from −5 V to +5 V. The linear relationship between the measured current and applied voltage of the synthesized gas sensors indicates that the contact between the electrode and the sensing materials is ohmic contact. Furthermore, with the decoration amount of Au nanoparticles increase, the resistance of Au/WS_2 nanocomposite-based sensors decreased, which is related to electrons transfer between WS_2 and Au nanoparticles due to the formation of heterostructures.

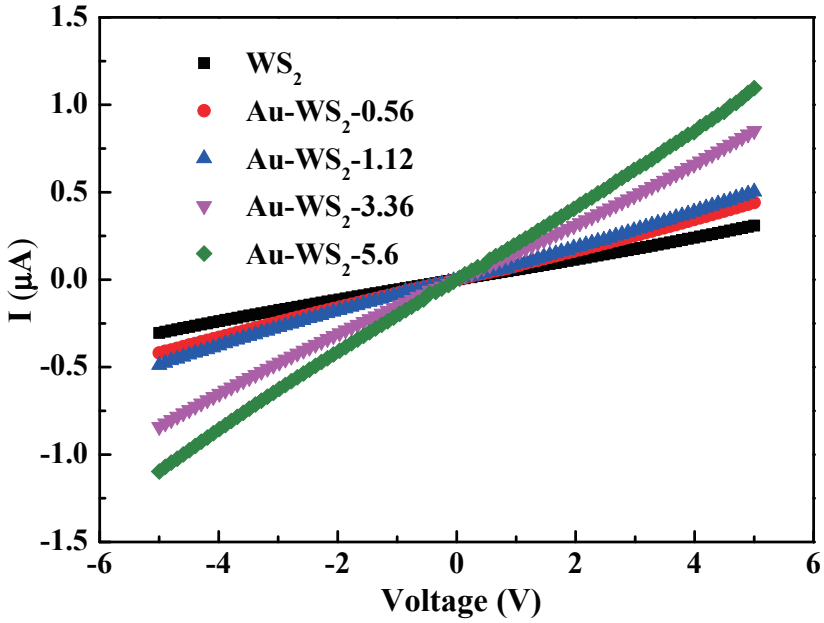

Figure 5. The polarization curves of the sensors using WS_2 and Au/WS_2.

The sensing properties of the fabricated WS_2 and Au/WS_2 sensors were investigated. Figure 6a shows the response of chemiresistive-type sensors to 10 ppm ammonia at room temperature. The sensors show an increase in resistance when exposed to NH_3, indicating a p-type response. With Au decoration, the WS_2 based sensors indicated a significantly improved response. The sensor using WS_2 microflakes decorated with 1.12 wt% Au achieved the largest response (723%), which is about 2.5 times higher than that of the pure one. Moreover, the sensor using WS_2 microflakes decorated with 5.6 wt% Au achieved a response of 452%, which is about 1.5 times higher than the pure one. The response and recovery times of the sensors to 10 ppm NH_3 are summarized in Figure 6b. This indicates that as the concentration of decorated Au nanoparticles in Au/WS_2 increases further up to 5.6 wt%, the response/recovery speeds of the Au/WS_2-5.6-based sensor improved, although the response decreased compared to the Au/WS_2-1.12-based one. However, the fast response/recovery features at room temperature are desirable for applications in some real scenes. For example, when the sensor was used in detecting ammonia in humid human breath, the sensor should have a fast response to ammonia to avoid more errors due to possible sticking of more ammonia molecule to the wall of the gas sampling bag and possible leakage of the sampled gas as sampling time progressed. It also needs a faster recovery speed with respect to the sensor in order to retain a quick measuring rate. Beyond room temperature, the response of the Au/WS_2-5.6 nanocomposite-based sensor to 10 ppm NH_3 dropped below 150%, which is lower than that of the sensor working at room temperature, as shown in Figure S6. Compared with other WS_2 and TMDs-based sensors, the Au/WS_2 nanocomposite-based sensor exhibited an excellent performance to ammonia, as shown in Table 1.

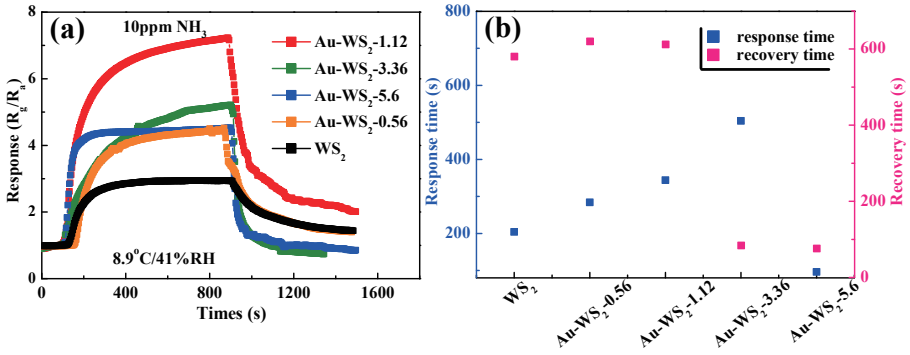

Figure 6. (**a**) Pure WS_2 and Au/WS_2 gas sensors response to 10 ppm NH_3 at room temperature; (**b**) the as-fabricated gas sensors response and recovery times to 10 ppm NH_3.

Table 1. A comparison of the performance of NH_3 sensors based on WS_2 and TMDs materials.

Sensitive Material	NH_3 Concentration	Temperature (°C)	Response (%)	Response/Recovery (s/s)	Ref.
WS_2/WO_3	10 ppm	150	400	~150/~100	[16]
WS_2 nanoflakes	5 ppm	RT	217[a]	120/150	[28]
Pt QDs/WS_2	250 ppm	RT	9.5[a]	200/1200	[30]
rGO/WS_2	10 ppm	RT	71	240/600	[36]
Mixed-phase WS_2	100 ppm	150	4.72	19/33	[37]
Flower-shaped SnS_2	100 ppm	200	7.4	40.6/624	[20]
2D SnS_2	500 ppm	RT	4.2	16/450	[21]
Au/WS_2	10 ppm	RT	452	96/76	This work

Data deduced from the reported figure; QDs: Quantum dots; rGO: Reduced graphene oxides; RT: Room temperature.

As a p-type semiconductor, there would be less charge carriers when the surface coverage of phisisorbed oxygen is decreased by the presence of a reducing species such as ammonia [36]. When exposed to NH_3, the resistance of the sensor based on WS_2 increased indicating a typical p-type character at room temperature. Moreover, the sensing process follows the proposed steps: the surface absorption of gas species and the desorption of reaction products according to the following reactions [38].

$$O_2(air) \rightarrow O_2(ads) \quad (2)$$

$$O_2(ads) + e^- \rightarrow O_2^-(ads)(\text{below } 100\,^\circ\text{C}) \quad (3)$$

$$4NH_3 + 5O_2^- \rightarrow 4NO + 6H_2O + 5e^- \quad (4)$$

As shown in Figure 7a(I), when the WS_2-based sensor is exposed in air, oxygen molecules are absorbed on the surface of WS_2 microflakes according to Equation (2). They will capture electrons from the conducting band of WS_2 to form oxygen ions resulting in an increase in the concentration of the majority carriers (holes) according to Equation (3). When the WS_2-based sensor is presented in NH_3 ambient (Figure 7b(I)), ammonia molecules react with the oxygen ions to form nitric oxide, water and free electrons, according to Equation (4). The produced electrons returned back to the conducting band of WS_2, which resulted in a decrease in the concentration of holes, resulting in an increase in the resistance of the WS_2-based sensor (Figure 7c(I)). Compared to pure WS_2 microflakes, the enhanced gas sensing mechanism of WS_2 decorated by gold nanoparticles can be suggested as the following two aspects. Firstly, enhanced sensing performance is related to the "electronic sensitization" effect between Au and WS_2. As illustrated in Figure 7c(II), as contact formed between Au and WS_2, the electrons in the conduction band of WS_2 microflakes would transfer to Au nanoparticles due to the higher Fermi level of WS_2 microflakes than that of Au nanoparticles [39,40]. Therefore, the entire accumulation

layer (HAL) is created at the interface of Au and WS_2, resulting in an increase in the concentration of holes in Au/WS_2 nanocomposites. Therefore, the initial resistance of the Au/WS_2-based sensor will be reduced, which is exhibited in Figure 7c(I), and this is beneficial to the enhancement of sensing responses according to the definition of sensing response ($R_s = R_g/R_a$). Secondly, the enhanced sensing performance is also related to the "chemical sensitization" effect of Au [41,42]. Due to the fact that the catalytic effect of Au nanoparticles can lower the enthalpy change of gas decomposition, the sensing reaction at room temperature will be enhanced, and absorption/desorption processes will be accelerated [13]. Furthermore, the formation of heterostructure between WS_2 and Au contributes an abundance of electrons assembled on Au nanoparticles, which will provide more active sites for more oxygen molecules due to the spillover effect of Au (Figure 7a(II)). The additional physisorbed oxygen ions on the surface of Au/WS_2 nanocomposites can be verified in O 1s core spectra in Figure 4c. Moreover, in NH_3 ambient (Figure 7b(II)), the existence of a high number of oxygen ions will facilitate surface sensing reactions. More NH_3 molecules will react with the absorbed oxygen ions, which results in more electrons injected back into WS_2 microflakes. As a result, there will be a thinner HAL at the interface of Au and WS_2 in Au/WS_2 nanocomposites, which will result in a greater increase in resistance of the sensor displayed in Figure 7c(I). In addition, the excellent chemical sensitization effect of Au nanoparticles can accelerate absorption/desorption processes, as shown in Figure 6b. Consequently, under the synergistic effect of electronic sensitization and chemical sensitization between WS_2 and Au, Au/WS_2-based sensors exhibit a higher response to ammonia and shorter response/recovery time than the pure WS_2-based sensor.

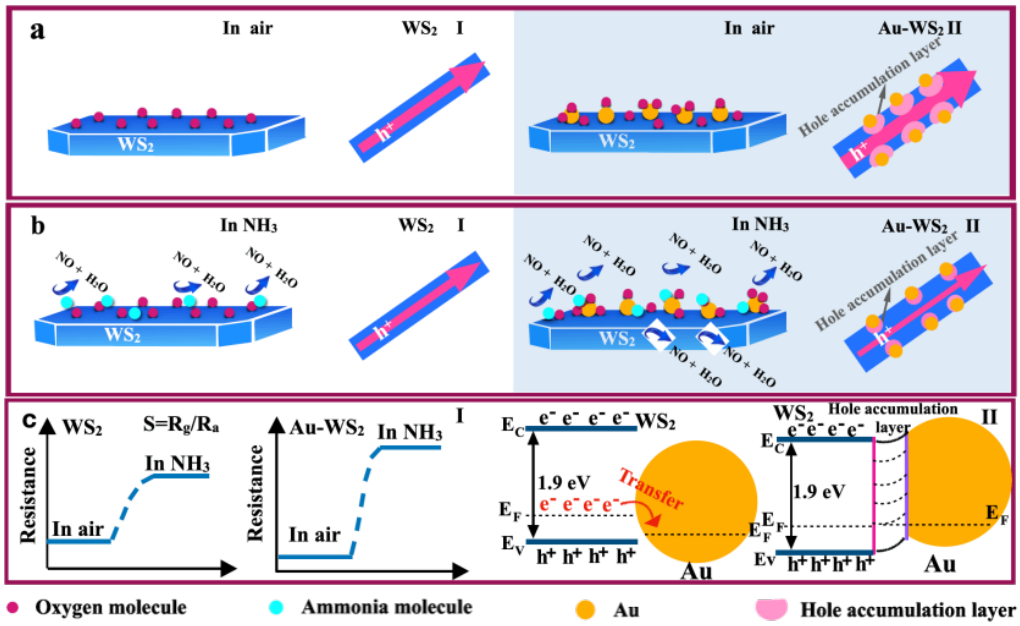

Figure 7. Schematic diagram of the pure WS_2 and Au/WS_2 sensors exposed to air and ammonia gas. (**a**) pure WS_2 sensors in air and ammonia gas (**b**) Au/WS_2 sensors in air and ammonia gas (**c**) pure WS_2 and Au/WS_2 sensors in air and ammonia gas

Figure 8a shows the response curves of pure WS_2, Au/WS_2-1.12 and Au/WS_2-5.6-based sensors to different concentrations of NH_3 from 1 ppm to 10 ppm at room temperature. Compared with the pure WS_2-based sensor, Au/WS_2-1.12 and Au/WS_2-5.6-based sensors exhibited higher responses to different concentration of ammonia. The correlations between sensor response and NH_3 concentrations were plotted in Figure 8b. As the ammonia concentration increased, the responses of the sensors increased. The responses of the sensors increased almost linearly with the increase in NH_3 concentrations. However, the slope of the Au/WS_2-1.12 sensor is higher than the pure WS_2 sensor, indicating better gas detection capability. The lower signals of the Au/WS_2 sensors with higher gold loading

(5.6 wt%) to NH_3 may result from "localized" NH_3 consumption without generation of electrons that would transfer to the conduction band of WS_2. In this case, Au acted as a "good catalyst" and the catalytic oxidation of ammonia would partly occur locally on gold nanoparticles. The induced charge transfer took place only in a localized manner and had no direct impact on the electrical conduction of WS_2. Similar observations are also found in literature [30,43].

Figure 8c shows the repeatability of the response of Au/WS_2-5.6 to 5 ppm NH_3 at room temperature. The response of the sensor maintained a stable line shape after 5-cycling measurements, indicating good repeatability of the sensor. A longer period of stability of the sensor for 30 days was studied by measuring the sensing performance of the sensor periodically. The signals remained pretty well within a variation error less than 3% after a 30-day operation, as shown in Figure 8d. Moreover, it shows excellent long term stability.

The selectivity of the sensor using Au/WS_2-5.6 was examined. Figure 9a shows that the developed sensor has a negligible response to several potential interference such as formaldehyde, benzene, acetone and ethanol with a concentration of 10 ppm each, indicating possible excellent selectivity. The dependency of the Au/WS_2-5.6-based sensor response on humidity was examined, and the results are shown in Figure 9b. The results indicated that the sensor could yield the maximum response when the RH was around 50%. The sensor was resistant to humidity and could work in a highly humid background. The sensor did not show much poisoning when operating at different humidities, as shown in Figure 9b. Sensor response decreased at RH beyond 55%; however, it recovered when RH changed to 55% again.

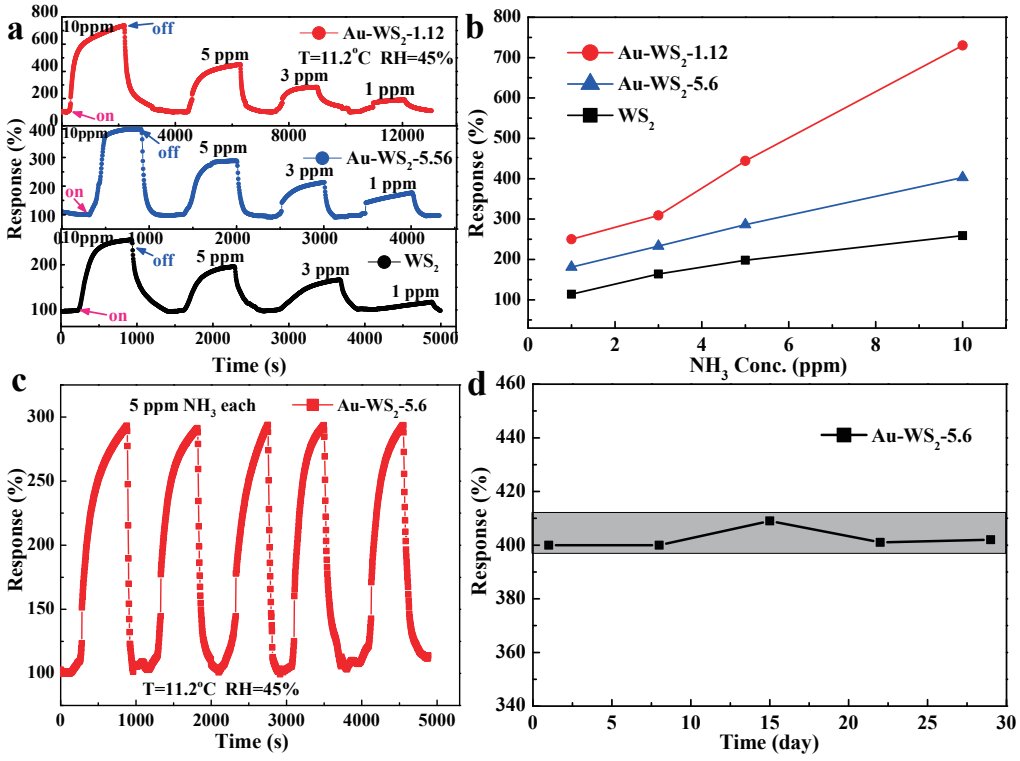

Figure 8. (**a**,**b**) Gas sensor responses to different concentrations of ammonia of Au/WS_2-1.12, Au/WS_2-5.56 and pure WS_2; (**c**) repeatability of gas sensor response to 5 ppm ammonia; (**d**) long-term stability of Au/WS_2-5.6-based gas sensor.

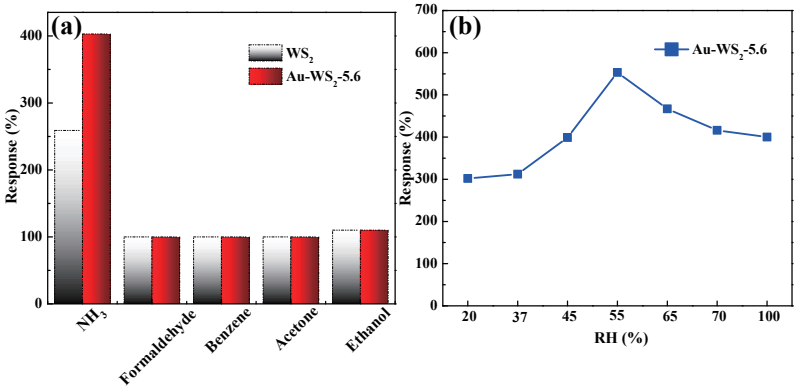

Figure 9. (**a**) Selectivity of the Au/WS_2-5.6 nanocomposite-based gas sensor to different gases at RH = 45%; (**b**) dependency of the sensor response on humidity.

4. Conclusions

Gold nanoparticles were decorated on WS_2 microflakes using an in situ chemical reduction route. The WS_2 nanoflakes' diameters are 0.4–4.3 micrometers and the diameters of the decorated Au nanoparticles are 17.8–48.8 nm. It was found that Au/WS_2 nanocomposite-based gas sensors present a higher response and faster response and recovery speeds relative to different concentrations of ammonia from 1 to 10 ppm. Moreover, the Au/WS_2-5.6 based sensor also displayed excellent selectivity relative to several typical interferents such as formaldehyde, benzene, acetone and ethanol. Gold nanoparticles loaded on the surface of WS_2 microflakes promoted sensing reactions, resulting in the improvement of gas-sensing properties due to the synergistic effect of electronic sensitization and chemical sensitization between WS_2 and Au.

Supplementary Materials: The following are available online at https://www.mdpi.com/article/10.3390/chemosensors10010009/s1.

Author Contributions: Conceptualization, Q.G.; methodology, Q.G.; validation, Q.G., B.H. and X.L.; formal analysis, Q.G.; investigation, Q.G.; writing—original draft preparation, Q.G.; writing—review and editing, B.H. and X.L.; supervision, X.L.; project administration, X.L.; funding acquisition, B.H. and X.L. All authors have read and agreed to the published version of the manuscript.

Funding: The authors are thankful to the National Key R&D Program of China (No. 2021YFB3201302), National Natural Science Foundation of China (No. 61971085, 62111530055) and the Fundamental Research Funds for the Central Universities (Nos: DUT19RC(3)054) for financial support.

Institutional Review Board Statement: Not applicable.

Informed Consent Statement: Not applicable.

Data Availability Statement: Not applicable.

Acknowledgments: The authors are thankful to the National Key R&D Program of China (No. 2021YFB3201302), National Natural Science Foundation of China (No. 61971085, 62111530055) and the Fundamental Research Funds for the Central Universities (Nos: DUT19RC(3)054) for financial support.

Conflicts of Interest: The authors declare no conflict of interest.

Sample Availability: Samples of compounds are available from the authors.

Abbreviations

The following abbreviations are used in this manuscript:

SCR	Selective catalytic reduction;
2D	Two-dimensional;
TMDs	Transitional metal dichalcogenides;

QDs	Quantum dots;
rGO	Reduced graphene oxides;
CNFs	Carbon nanofibers;
XRD	X ray diffractometer;
FESEM	Field emission scanning electronic microscope;
TEM	Transmission electron microscope;
HRTEM	High resolution transmission electron microscope;
EDS	Energy dispersive X-ray spectroscopy;
XPS	X-ray photoelectron spectra;
RT	Room temperature;
HAL	Hole accumulation layer.

References

1. Aslam, M.; Chaudhary, V.A.; Mulla, I.S.; Sainkar, S.R.; Mandale, A.B.; Belhekar, A.A.; Vijayamohanan, K. A highly selective ammonia gas sensor using surface-ruthenated zinc oxide. *Sens. Actuators A Phys.* **1999**, *75*, 162–167. [CrossRef]
2. Schönauer, D.; Wiesner, K.; Fleischer, M.; Moos, R. Selective mixed potential ammonia exhaust gas sensor. *Sens. Actuators B Chem.* **2009**, *140*, 585–590. [CrossRef]
3. Buckley, S.G.; Damm, C.J.; Vitovec, W.M.; Sgro, L.A.; Sawyer, R.F.; Koshland, C.P.; Lucas, D. Ammonia detection and monitoring with photofragmentation fluorescence. *Appl. Opt.* **1998**, *37*, 8382–8391. [CrossRef]
4. Timmer, B.; Olthuis, W.; Berg, A.V.D. Ammonia sensors and their applictions-a review. *Sens. Actuators B Chem.* **2005**, *107*, 666–677. [CrossRef]
5. Miller, D.R.; Akbar, S.A.; Morris, P.A. Nanoscale metal oxide-based heterojunctions for gas sensing: A review. *Sens. Actuators B Chem.* **2014**, *204*, 250–272. [CrossRef]
6. Li, X.; Li, X.; Wang, J.; Lin, S. Highly sensitive and selective room-temperature formaldehyde sensors using hollow TiO_2 microspheres. *Sens. Actuators B Chem.* **2015**, *219*, 158–163. [CrossRef]
7. Qin, Z.; Zeng, D.; Zhang, J.; Wu, C.; Wen, Y.; Shan, B.; Xie, C. Effect of layer number on recovery rate of WS_2 nanosheets for ammonia detection at room temperature. *Appl. Surf. Sci.* **2017**, *414*, 244–250. [CrossRef]
8. Zhou, Y.; Liu, G.; Zhu, X.; Guo, Y. Ultrasensitive NO_2 gas sensing based on rGO/MoS_2 nanocomposite film at low temperature. *Sens. Actuators B Chem.* **2017**, *251*, 280–290. [CrossRef]
9. Lu, G.; Ocola, L.E.; Chen, J. Reduced graphene oxide for room-temperature gas sensors. *Nanotechnology* **2009**, *20*, 445502. [CrossRef]
10. Geim, A.K.; Novoselov, K.S. The rise of graphene. *Nat. Mater.* **2007**, *6*, 183–191. [CrossRef]
11. Kim, Y.H.; Phan, D.T.; Ahn, S.; Nam, K.H.; Park, C.M.; Jeon, K.J. Two-dimensional SnS_2 materials as high-performance NO_2 sensors with fast response and high sensitivity. *Sens. Actuators B Chem.* **2018**, *255*, 616–621. [CrossRef]
12. Dai, L.; Huang, K.; Xia, Y.; Xu, Z. Two-dimensional material separation membranes for renewable energy purification, storage, and conversion. *Green Energy Environ.* **2021**, *6*, 193–211. [CrossRef]
13. Huang, B.; Wang, Y.; Hu, Q.; Mu, X.; Zhang, Y.; Bai, J.; Wang, Q.; Sheng, Y.; Zhang, Z.; Xie, E. A low temperature and highly sensitive ethanol sensor based on Au modified In_2O_3 nanofibers by coaxial electrospinning. *J. Mater. Chem. C* **2018**, *6*, 10935–10943. [CrossRef]
14. Zhang, X.; Liu, Y.; Chen, L.; Li, Z.; Qu, Y.; Wu, W.; Jing, L. Porous two-dimension MnO_2-C_3N_4/titanium phosphate nanocomposites as efficient photocatalsyts for CO oxidation and mechanisms. *Appl. Catal.* **2021**, *282*, 119563. [CrossRef]
15. Cheng, M.; Wu, Z.; Liu, G.; Zhao, L.; Gao, Y.; Zhang, B.; Liu, F.; Yan, X.; Liang, X.; Sun, P.; et al. Highly sensitive sensors based on quasi-2D rGO/SnS_2 hybrid for rapid detection of NO_2 gas. *Sens. Actuators B Chem.* **2019**, *291*, 216–225. [CrossRef]
16. Perrozzi, F.; Emamjomeh, S.M.; Paolucci, V.; Taglieri, G.; Ottaviano, L.; Cantalini, C. Thermal stability of WS_2 flakes and gas sensing properties of WS_2/WO_3 composite to H_2, NH_3 and NO_2. *Sens. Actuators B Chem.* **2017**, *243*, 812–822. [CrossRef]
17. Chen, Y.; Pei, Y.; Jiang, Z.; Shi, Z.; Xu, J.; Wu, D.; Xu, T.; Tian, Y.; Wang, X.; Li, X. Humidity sensing properties of the hydrothermally synthesized WS_2-modified SnO_2 hybrid nanocomposite. *Appl. Surf. Sci.* **2018**, *447*, 325–330. [CrossRef]
18. Zhang, X.; Wang, J.; Chen, D.; Liu, L. The adsorption performance of harmful gas on Cu doped WS_2: A first-principle study. *Mater. Today Commun.* **2021**, *28*, 102488. [CrossRef]
19. Nguyen, T.K.; Jeong, S.; Youn, J.S.; Ahn, S.; Nam, K.H.; Park, C.M.; Jeon, K.J. Insight into mechanism of temperature-dependent limit of NO_2 detection using monolayer MoS_2. *Sens. Actuators B Chem.* **2021**, *329*, 129138. [CrossRef]
20. Xiong, Y.; Xu, W.; Ding, D.; Lu, W.; Zhu, L.; Zhu, Z.; Wang, Y.; Xue, Q. Ultra-sensitive NH_3 sensor based on flower-shaped SnS_2 nanostructures with sub-ppm detection ability. *J. Hazard. Mater.* **2018**, *341*, 159–167. [CrossRef]
21. Qin, Z.; Xu, K.; Yue, H.; Wang, H.; Zhang, J.; Ouyang, C.; Xie, C.; Zeng, D. Enhanced room-temperature NH_3 gas sensing by 2D SnS_2 with sulfur vacancies synthesized by chemical exfoliation. *Sens. Actuators B Chem.* **2018**, *262*, 771–779. [CrossRef]
22. Wang, L.; Fu, H.; Jin, Q.; Jin, H.; Haick, H.; Wang, S.; Yu, K.; Deng, S.; Wang, Y. Directly transforming SnS_2 nanosheets to hierarchical SnO_2 nanotubes: Towards sensitive and selective sensing of acetone at relatively low operating temperatures. *Sens. Actuators B Chem.* **2019**, *292*, 148–155. [CrossRef]

23. Radisavljevic, B.; Radenovic, A.; Brivio, J.; Giacometti, V.; Kis, A. Single-layer MoS_2 transistors. *Nat. Nanotechnol.* **2011**, *6*, 147–150. [CrossRef] [PubMed]
24. Yan, W.; Worsley, M.A.; Pham, T.; Zettl, A.; Carraro, C.; Maboudian, R. Effects of ambient humidity and temperature on the NO_2 sensing characteristics of WS_2/graphene aerogel. *Appl. Surf. Sci.* **2018**, *450*, 372–379. [CrossRef]
25. Agrawal, A.V.; Kumar, R.; Yang, G.; Bao, J.; Kumar, M. Enhanced adsorption sites in monolayer MoS_2 pyramid structures for highly sensitive and fast hydrogen sensor. *Int. J. Hydrogen Energy* **2020**, *45*, 9268–9277. [CrossRef]
26. Shokri, A.; Salami, N. Gas sensor based on MoS_2 monolayer. *Sens. Actuators B Chem.* **2016**, *236*, 378–385. [CrossRef]
27. Cui, S.; Wen, Z.; Huang, X.; Chang, J.; Chen, J. Stabilizing MoS_2 Nanosheets through SnO_2 Nanocrystal Decoration for High-Performance Gas Sensing in Air. *Small* **2015**, *11*, 2305–2313.
28. Li, X.; Li, X.; Li, Z.; Wang, J.; Zhang, J. WS_2 nanoflakes based selective ammonia sensors at room temperature. *Sens. Actuators B Chem.* **2017**, *240*, 273–277. [CrossRef]
29. Gu, D.; Li, X.; Wang, H.; Li, M.; Xi, Y.; Chen, Y.; Wang, J.; Rumyntseva, M.N.; Gaskov, A.M. Light enhanced VOCs sensing of WS_2 microflakes based chemiresistive sensors powered by triboelectronic nangenerators. *Sens. Actuators B Chem.* **2018**, *256*, 992–1000. [CrossRef]
30. Ouyang, C.; Chen, Y.; Qin, Z.; Zeng, D.; Zhang, J.; Wang, H.; Xie, C. Two-dimensional WS_2-based nanosheets modified by Pt quantum dots for enhanced room-temperature NH_3 sensing properties. *Appl. Surf. Sci.* **2018**, *455*, 45–52. [CrossRef]
31. Xu, Y.; Xie, J.; Zhang, Y.; Tian, F.H.; Yang, C.; Zheng, W.; Liu, X.; Zhang, J.; Pinna, N. Edge-enriched WS_2 nanosheets on carbon nanofibers boosts NO_2 detection at room temperature. *J. Hazard. Mater.* **2021**, *411*, 125120. [CrossRef] [PubMed]
32. Suh, J.M.; Kwon, K.C.; Lee, T.H.; Kim, C.; Lee, C.W.; Song, Y.G.; Choi, M.J.; Choi, S.; Cho, S.H.; Kim, S.; et al. Edge-exposed WS_2 on 1D nanostructures for highly selective NO_2 sensor at room temperature. *Sens. Actuators B Chem.* **2021**, *333*, 129566. [CrossRef]
33. Liu, W.; Gu, D.; Li, X. AuPt Bimetal-Functionalized $SnSe_2$ Microflower-Based Sensors for Detecting Sub-ppm NO_2 at Low Temperatures. *ACS Appl. Mater. Interfaces* **2021**, *13*, 20336–20348. [CrossRef] [PubMed]
34. Liu, W.; Gu, D.; Li, X. Detection of Ppb-level NO_2 using mesoporous ZnSe/SnO_2 core-shell microspheres based chemical sensors. *Sens. Actuators B Chem.* **2020**, *320*, 128365. [CrossRef]
35. Liu, W.; Gu, D.; Zhang, J.W.; Li, X.G.; Rumyantseva, M.N.; Gaskov, A.M. ZnSe/NiO heterostructure-based chemiresistive-type sensors for low-concentration NO_2 detection. *Rare Met.* **2021**, *40*, 1632–1641. [CrossRef]
36. Wang, X.Y.; Gu, D.; Li, X.; Lin, S.; Zhao, S.; Rumyantseva, M.N.; Gaskov, A.M. Reduced graphene oxide hybridized with WS_2 nanoflakes based heterojunctions for selective ammonia sensors at room temperature. *Sens. Actuators B Chem.* **2019**, *282*, 290–299. [CrossRef]
37. Meng, F.; Zhu, T.; Yuan, Z.; Qin, W.; Gao, H.; Zhang, H. Investigation of Mixed-Phase WS_2 Nanomaterials for Ammonia Gas Sensing. *IEEE Sens. J.* **2021**, *21*, 7268–7274. [CrossRef]
38. Sharma, N.; Sharma, N.; Srinivasan, P.; Kumar, S.; Rayappan, J.B.B.; Kailasam, K. Heptazine based organic framework as a chemiresistive sensor for ammonia detection at room temperature. *J. Mater. Chem. A* **2018**, *6*, 18389–18395. [CrossRef]
39. Kim, J.H.; Mirzaei, A.; Kim, H.W.; Kim, S.S. Realization of Au-decorated WS_2 nanosheets as low power-consumption and selective gas sensors. *Sens. Actuators B Chem.* **2019**, *296*, 126659. [CrossRef]
40. Zhang, S.; Song, P.; Zhang, J.; Yan, H.; Li, J.; Yang, Z.; Wang, Q. Highly sensitive detection of acetone using mesoporous In_2O_3 nanospheres decorated with Au nanoparticles. *Sens. Actuators B Chem.* **2017**, *242*, 983–993. [CrossRef]
41. Zhang, S.; Song, P.; Yan, H.; Wang, Q. Self-assembled hierarchical Au-loaded In_2O_3 hollow microspheres with superior ethanol sensing properties. *Sens. Actuators B Chem.* **2016**, *231*, 245–255. [CrossRef]
42. Fu, H.; Hou, C.; Gu, F.; Han, D.; Wang, Z. Facile preparation of rod-like Au/In_2O_3 nanocomposites exhibiting high response to CO at room temperature. *Sens. Actuators B Chem.* **2017**, *243*, 516–524. [CrossRef]
43. Zeb, S.; Peng, X.; Shi, Y.; Su, J.; Sun, J.; Zhang, M.; Sun, G.; Nie, Y.; Cui, Y.; Jiang, X. Bimetal Au-Pd decorated hierarchical WO_3 nanowire bundles for gas sensing application. *Sens. Actuators B Chem.* **2021**, *334*, 129584. [CrossRef]